2.F: 2.L

Nuclear Physics **74** (1965) 481—496; © *North-Holland Publishing Co., Amsterdam*

ELASTIC SCATTERING OF 27.5 MeV DEUTERONS AND ITS OPTICAL MODEL ANALYSIS

J. TESTONI, J. ROSENBLATT and S. MAYO

Comisión Nacional de Energía Atómica, Buenos Aires, Argentina †

Received 14 April 1965

Abstract: Absolute differential cross-sections for elastic scattering of 27.5 MeV deuterons by Mg, V, Fe, ^{58}Ni, Co, ^{65}Cu, Ag, Au and ^{208}Pb were measured from 15° to 140°. The data were analysed in terms of a surface absorption optical model. Some sets of parameters giving good fits to the data show definite dependence on mass number.

E NUCLEAR REACTIONS Mg, V, Fe, ^{58}Ni, Co, ^{65}Cu, Ag, Au, ^{208}Pb(d, d), $E = 27.5$ MeV; measured $\sigma(\theta)$.

1. Introduction

Different studies have shown the possibility of extending the optical model description of elastic scattering to complex particles [1]). In the case of deuterons, parameter sets which fit the experimental data for a range of target nuclei and energies between 3 and 27.5 MeV have been obtained in recent surveys [2, 3]). Furthermore, measurements of elastic differential cross-sections [4]), polarization [5]) and total reaction cross-sections [6]) have become available.

A distinctive feature of differential cross-section analyses is the appearance of discrete families of parameter sets which fit the experimental data almost equally well. It has been shown [3]) that these families result from a similar behaviour for different parameter sets of the most important l waves at the surface of the nucleus. Moreover Drisko *et al.* [7]) have shown that such effects could be understood in terms of a discrete ambiguity between the real and imaginary potentials. Such families of potentials have also appeared in the optical model study of proton scattering [8]). In that case it is easy to select the proper one from the requirement that the real potential should smoothly join the values used in the shell model of the nucleus. A condition of this type is not available for deuterons. It might also be mentioned that nuclear radii for optimum fits in some optical model analyses of deuteron data tend to be smaller than those usual in the nucleon case, in spite of the extended structure of the deuteron.

The aim of the present work has been to extend the measurements of elastic dis-

† Work sponsored in part by Consejo Nacional de Investigaciones Científicas y Técnicas, Argentina.

tributions at 27.5 MeV to a number of nuclei and to find out whether trends and correlations exist among the optical model parameters fitting the data.

In fact, the answer to the latter problem need not be unique when a limited amount of data is available. No less important, is the fact that it is almost impossible to conduct a bias-free search. Given a criterion for goodness of fit, the initial values of the parameters, the order and number in which they are varied, the estimated experimental errors and the density of experimental data, in conjunction with the many ambiguities of the model, very markedly influence the final result. With these limitations, the tendencies observed here for the different parameters can be said to be compatible with a reasonable fit to the data, but not to follow uniquely from the latter.

2. Experimental Procedure

The experimental set-up was similar to that described previously [4]). Metallic targets of natural Mg, V, Fe, Co, Ag and Au and isotopically enriched ^{58}Ni, ^{65}Cu and ^{208}Pb were used †. The incident beam energy was 27.5 ± 0.1 MeV. The energy loss in the targets was between 1 and 2 %. Measurements were done between 15° and 140° every 5° in the forward hemisphere and every 10° in the backward hemisphere. A NaI(Tl) scintillator mounted on a Philips 53 AVP photomultiplier was used to detect the scattered deuterons. The pulses were fed into a Nuclear Data Model 120 pulse-height analyser.

An energy resolution of 3 % or better was achieved. Possible contributions from first excited levels of V, Ag and Au were assumed to be unimportant.

The experimental angular distributions are shown in fig. 1 together with optical model fits (see below). The experimental errors shown include contributions from statistics, background subtraction, determination of the number of target atoms, charge collection and measurement of solid angle.

3. Optical Model Analysis

3.1. OPTICAL POTENTIALS

The optical potential used in this work is a sum of a real refractive volume term

$$-Uf(r),$$

an imaginary absorptive surface term

$$-iWg(r),$$

and the Coulomb potential

$$(\tfrac{1}{2}Ze^2/R_C)[3-(r/R_C)^2] \text{ for } r \leqq R_C, \qquad Ze^2/r \text{ for } r \geqq R_C,$$

that would be produced by a uniformly charged sphere of radius $R_C = r_C A^{\frac{1}{3}}$.

† The ^{208}Pb was obtained from Oak Ridge National Laboratory.

The function $f(r)$ is a Saxon-Woods form factor

$$f(r) = \{1+\exp[(r-r_u A^{\frac{1}{3}})/a_u]\}^{-1},$$

and $g(r)$ is a Gaussian form factor

$$g(r) = \exp[(r-r_w A^{\frac{1}{3}})/a_w]^2.$$

Spin-orbit terms are not included in these calculations.

The calculations were carried out on the Mercury computer of the University of Buenos Aires. The programme included a least-squares automatic search code which sought to minimize the quantity

$$\Delta = \sum_{i=1}^{N} [\sigma_{th}(\theta_i)-\sigma_{exp}(\theta_i)]^2/[\delta(\theta_i)]^2,$$

by systematic variation of the parameters. In the above equation, N is the number of experimental points, $\sigma_{th}(\theta_i)$ and $\sigma_{exp}(\theta_i)$ are the predicted and experimental cross-sections at angle θ_i; $\sigma(\theta_i)$ are the errors attached to each point. No normalization factors were used.

In the early steps of the analysis the values of $\delta(\theta_i)$ were set equal to the experimental errors. The first runs, made on medium-weight nuclei, gave reasonably good fits to the experimental cross-sections in the forward angles but, as a rule, the predictions were too small at backward angles. Nevertheless, some parameter sets were obtained that showed the ability of the model to give a satisfactory fit to the whole angular distribution.

It would seem that the relatively large experimental errors, smaller cross-sections and lower density of experimental points usually associated with the backward hemisphere result in biassing the search toward smaller angles. It was therefore decided to make

$$\delta(\theta_i) = 0.1\ \sigma_{exp}(\theta_i)$$

at all points, which is not far away from the average experimental situation. In this way an over-all agreement with the data was the usual result of the search.

In order to facilitate comparison of optical model predictions for different nuclei the quantity

$$\xi^2 = \frac{\Delta}{N}$$

is used in this paper as figure of merit of the different fits.

Most of the work reported here concerns the two-nucleon family [2]) (i.e., parameter sets where the real potential is roughly equal to the sum of proton and neutron potentials). A few calculations were carried out with parameter sets belonging to the one-nucleon family. It has been pointed out [9]) that the two-nucleon parameter sets may have a greater physical appeal.

3.2. ANALYSIS IN MODE I

As mentioned in sect. 1, many ambiguities, both continuous and discrete, arise when deuteron data are analysed in terms of the optical model. Moreover, it has been noticed before [3]) that the quality of the fits worsens at higher energies, where the angular distributions have a more pronounced structure. This is particularly true at the energy at which our data were obtained. As a result of both effects the convergence of a given search becomes slower and the parameters obtained are not uniquely defined.

The aim of this analysis was to determine the possible existence of trends in the individual parameters as functions of nuclear properties. For the reasons stated above the task of extricating those tendencies out of a "free" (with the restrictions touched upon in sect. 1) six-parameter search on all nuclei appeared as a formidable one. It was decided instead to follow the procedure described below, which we shall call mode I.

A careful six-parameter search was carried out on the ^{58}Ni data, until a good fit was obtained. The resulting parameters were used as starting values to seek a good fit to the Ag and V data, the results of the latter being used in turn as a starting point for a search on Mg. In this way the ^{58}Ni parameters "radiated" as it were toward lighter and heavier nuclei. In all these searches U and W were varied first, keeping the remaining parameters constant until a reasonable fit was obtained. This was followed by a four- or five-parameter variation, according to whether the machine omitted the variation of one of the parameters. The calculations are programmed in such a way [10]) that this will happen automatically when an ambiguity is present. A further six-parameter variation usually did not lead to a significant improvement in the goodness-of-fit, although some changes in the parameters could be brought about.

The parameter values thus found were plotted as a function of the nuclear mass A and starting values for the remaining nuclei were found by interpolation or extrapolation, as the case might be.

These starting values gave as a rule a reasonable fit. A search was then made by varying r_w and a_w, keeping all other parameters fixed, until a good fit ($\xi^2 \approx 16$ for medium-weight nuclei) was obtained. The data for Mg, V and Ag were also re-examined following the same method, that is, variation of r_w and a_w only. The outcome of this search appears in table 1 as mode I. The optical model results are shown, together with the experimental data, in fig. 1.

3.3. TRENDS IN THE PARAMETERS

It is well known that the (local) optical potential is momentum-dependent. The potential well depth is therefore expected to vary smoothly with incident energy. In the case of charged particles it has been shown by Lane [11]) that a smooth variation with the Coulomb potential of the nucleus should also be expected. Assuming

TABLE 1

Results of the optical model analysis

Nucleus	Mode	U (MeV)	r_u (fm)	a_u (fm)	W (MeV)	r_w (fm)	a_w (fm)	ξ^2	σ_r (mb)	σ_r [b] (mb)
Mg	I	78.70	1.210	0.850	19.23	1.027	2.076	14.5	1275	1202±55
	I [a]	78.70	1.092	0.821	17.36	0.500	3.165	7.4	1308	
	III	80.00	1.230	0.798	20.00	0.912	2.280	17.1	1277	
	III [a]	86.50	1.129	0.898	20.00	0.910	2.280	12.3	1269	
^{51}V	I	81.80	1.225	0.790	21.50	1.342	1.375	22.7	1487	1631±49
	II	68.03	1.355	0.723	21.78	1.355	1.375	24.3	1533	
	III	81.80	1.230	0.824	21.50	1.360	1.356	21.6	1522	
Fe	II	75.66	1.269	0.761	20.20	1.269	1.547	16.6	1539	1676±46
	III	82.00	1.230	0.796	22.10	1.270	1.488	19.6	1526	
^{58}Ni	I	82.27	1.227	0.780	22.11	1.309	1.394	10.4	1494	1537±48
	II	75.52	1.293	0.747	23.09	1.293	1.380	12.3	1513	(natural Ni)
	III	82.26	1.229	0.790	22.10	1.293	1.421	11.1	1511	
^{59}Co	I	82.00	1.225	0.780	22.10	1.275	1.467	23.0	1530	1586±49
	I [a]	90.37	1.148	0.825	22.60	1.275	1.488	21.1	1522	
	II	77.30	1.251	0.736	19.18	1.251	1.710	21.2	1591	
	III	82.00	1.225	0.752	22.10	1.209	1.696	23.1	1556	
^{65}Cu	I	83.00	1.235	0.765	22.60	1.266	1.612	19.4	1642	1660±49
	II	69.80	1.365	0.725	22.43	1.365	1.349	24.7	1679	(Natural Cu)
	III	83.00	1.235	0.805	22.60	1.290	1.569	17.9	1675	
Ag	I	86.10	1.248	0.699	24.61	1.147	1.623	28.2	1727	1855±50
	II	100.09	1.137	0.738	15.91	1.137	2.047	20.9	1786	
	III	86.10	1.250	0.776	24.60	1.189	1.921	20.3	1976	
	III [a]	86.10	1.250	0.782	24.60	1.120	2.339	10.6	2139	
Au	I	89.00	1.265	0.620	27.40	0.936	2.899	5.0	2252	2028±65
	III	89.00	1.265	0.737	27.40	1.090	2.429	10.0	2324	
	III [a]	89.00	1.265	0.618	27.40	0.916	3.073	8.3	2345	
^{208}Pb	I	91.00	1.270	0.625	27.60	0.997	2.179	5.0	1978	2162±70
	I [a]	117.72	1.035	0.901	21.44	1.167	1.833	12.1	1939	
	I [a]	84.90	1.230	0.910	20.58	1.300	1.874	7.6	2422	
	III	91.00	1.265	0.517	27.60	0.517	4.032	5.7	2144	

[a]) Parameter sets obtained during the search in the modes indicated by the roman numerals, not shown in figs. 1–3 and 5.
[b]) Experimental reaction cross-sections from Mayo *et al.* [6]).

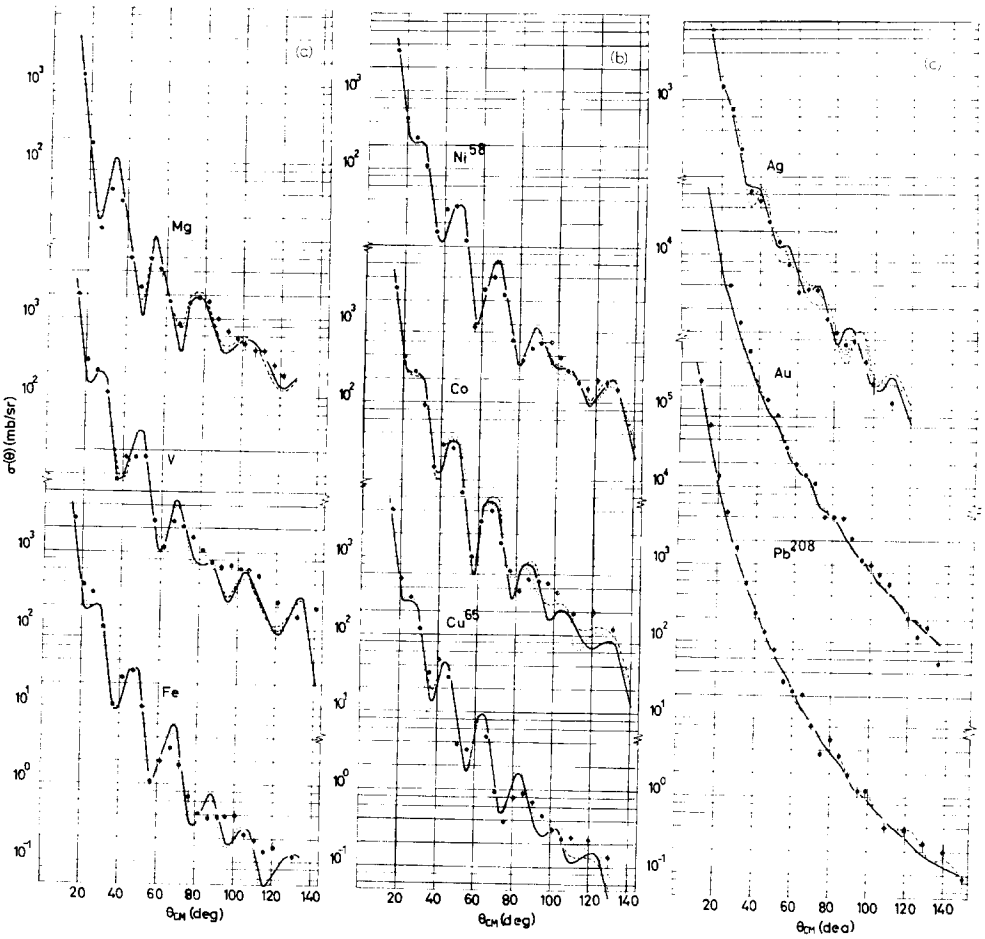

Fig. 1. Differential cross-sections and optical model fits of (a) Mg, V and Fe; (b) ^{58}Ni, Co and ^{65}Cu; (c) Ag, Au and ^{208}Pb. Dashed lines correspond to analysis in mode I (see the text), dotted lines to mode II and full lines to mode III.

a linear dependence upon kinetic energy, the expression for the optical potential becomes [12])

$$U = U_0 + \beta(V_C - E). \tag{1}$$

That is, U should vary with the Coulomb potential V_C in the same way as with total energy E. Perey [12]) has analysed proton data replacing V_C by its average over the nuclear volume $\overline{V}_C$. In this paper the value of the Coulomb potential V_{C0} at the centre of the nucleus has been adopted, on the grounds that the real well depth is also evaluated at the nuclear centre. The relation between both quantities is

$$\overline{V}_C = 0.8\ V_{C0},$$
$$V_{C0} = \tfrac{3}{2} Ze^2/R_C.$$

In fig. 2 the values of U and W have been plotted against V_{Co}. The values of V_{Co} were calculated from data published in tables [13]) of radii of equivalent charge distributions as obtained from electron scattering experiments. Both parameters show

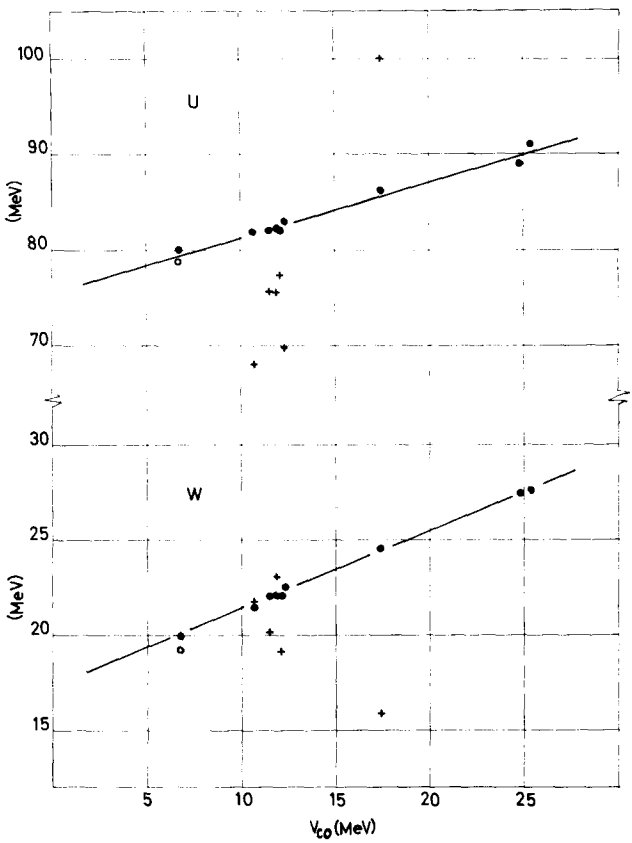

Fig. 2. Trends in the parameters U and W as functions of the Coulomb potential at the centre of the nucleus. Open circles correspond to mode I, crosses to mode II and full circles to mode III.

very similar trends. The straight line drawn through the U points satisfies the equation

$$U = 91.2+0.57(V_{Co}-27.5) \text{ MeV}. \quad (2)$$

The slope is therefore quite close to that obtained by Perey [12]) for the energy dependence of the proton potential when the coupling of low-lying levels to the ground state is not taken into account.

It has been customary to express the dependence on the Coulomb potential in terms of the quantity $Z/A^{\frac{1}{3}}$. A plot of the values of U against this quantity gives a slope of 1.03, which differs appreciably from the values obtained in a previous analysis [2]) of deuteron data using different sets of fixed geometrical parameters

(r_u, a_u, r_w and a_w). In the work reported here (see table 1), the geometrical parameters have not been kept fixed; r_u in particular increases smoothly with A. One might think that due to the ambiguity in the quantity $U-r_u$ a much steeper increase of U would have been obtained, had r_u been kept constant throughout the analysis. Nevertheless, as suggested by Gomes [14]), the observed trend in r_u can be made at least conceivable in terms of the extended structure of the deuteron. We shall approach this problem qualitatively by considering the deuteron as a sphere of radius d (fig. 4) where the probability of finding a nucleon is constant throughout the volume. Let the nucleus act on each nucleon as a square well potential of depth U_N and radius R_N. The potential acting on both nucleons, that is on the deuteron, will reach its full value when the deuteron is completely inside the nucleus. In other words,

$$U = 2U_N \text{ for } r \leqq R_N - d,$$

where r is the distance between both centres of mass. On the other hand

$$U = 0 \text{ for } r > R_N + d,$$

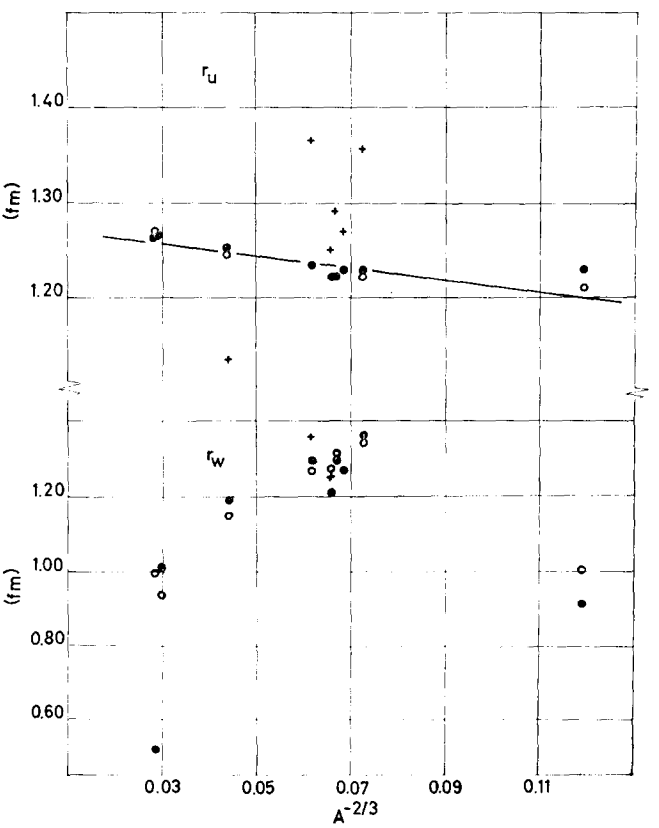

Fig. 3. Radius parameters r_u and r_w plotted against $A^{-\frac{2}{3}}$. Symbols for the different modes are the same as in fig. 2.

that is, when both nucleons are outside the nucleus. At intermediate points the potential will be proportional to the probability that a nucleon from the deuteron is inside the nuclear volume, which is in turn proportional to the volume intersected by both spheres, as shown in fig. 4.

The deuteron potential generated by square nucleon potentials varies therefore smoothly with radius, *acquiring a finite diffuseness.*

One should similarly expect that the diffuseness found in realistic deuteron analyses is appreciably greater than that appropriate for neutrons and protons; this is indeed the case.

The radius, i.e. the point at which the potential is half its maximum value, will also be affected. As can be seen from fig. 4, the intersected volume will be half that of the deuteron when the deuteron centre is already inside the nucleus. This effect will be less pronounced for heavier nuclei. More quantitatively, the radius for the deuteron potential can be shown to be

$$R_D = R_N - \tfrac{1}{2}d^2/R_N, \tag{3}$$

if $d^2/R_N^2 \ll 1$. Replacing $R_D = r_u A^{\frac{1}{3}}$, $R_N = r_N A^{\frac{1}{3}}$ in eq. (3),

$$r_u = r_N - \tfrac{1}{2}\frac{d^2}{r_N A^{\frac{1}{3}}}. \tag{3'}$$

Eq. (3') provides some justification for plotting r_u against $A^{-\frac{1}{3}}$, as has been done in fig. 3.

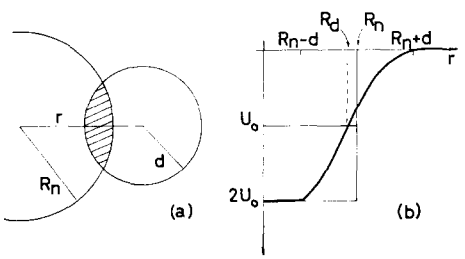

Fig. 4(a) Scattering of a "sharp" spherical deuteron by a square one-nucleon potential. (b) Deformed potential as seen by the deuteron.

The trend is similar to that predicted by eq. (3') although the slope corresponds to a rather small deuteron radius. This is understandable, since it should be expected that a diffuse one-nucleon potential should tend to smooth out the effect. Eq. (3') predicts values for r_u smaller than those suitable for proton and neutron analyses, tending to these values as A tends to infinity. An extrapolation of the line drawn in fig. 3 gives an intercept with the r_u-axis of 1.28 fm.

The pictorial description above corresponds to a quantal calculation of the deuteron potential as

$$U = \langle \varphi_d(1, 2) | U(1) + U(2) | \varphi_d(1, 2) \rangle,$$

where $U(1)$ and $U(2)$ are the nuclear potentials acting on the two particles thatform the deuteron, taken in this case as square-well potentials of depth U_N, and $\varphi_d(1, 2)$ is the deuteron ground-state wave function, which is taken as a square pulse.

The other parameters have also been plotted against $A^{-\frac{2}{3}}$ and show no marked trends with the exceptation of a_u (fig. 5). This parameter decreases steadily with increasing mass numbers. No explanation was found for this behaviour.

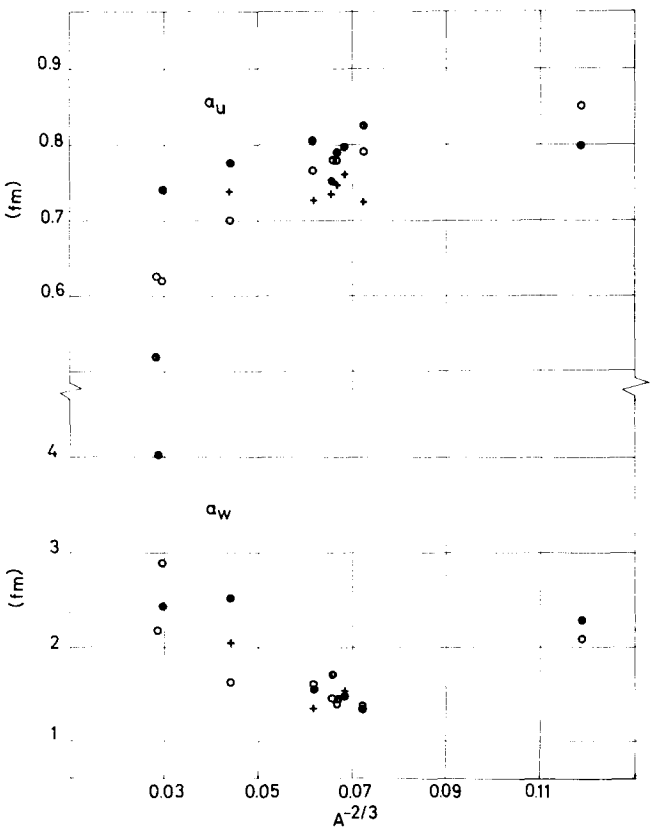

Fig. 5. Diffuseness parameters a_u and a_w plotted against $A^{-\frac{2}{3}}$. Symbols correspond to those of fig. 2.

3.4. ANALYSIS IN MODE II

The procedure outlined in the preceding subsection affected the values of all six parameters. It is well known, however, that a five-parameter search can also provide good fits to the data. In order to assess whether the trends resulting from mode I were maintained in a five-parameter search, the data were re-examined under the condition that $r_u = r_w$. The initial values for this search were determined as follows. The average of r_u and r_w as resulting from mode I was taken as the initial value for these parameters. The value of U was then suitably modified as suggested by the $U-r_u$ ambiguity. Values close to those abtained from mode I were adopted for the

remaining parameters. A reasonably good fit was the usual result of the initial set of parameters. This result allowed all five parameters to be varied simultaneously in the subsequent search.

The parameter values resulting from mode II also appear in table 1 and are plotted in figs. 2, 3 and 5.

The parameters are widely scattered, with no significant improvement in the goodness-of-fit with respect to mode I. It is worth noting that the analysis performed in mode II is considerably less biassed as regards smoothness of parameter change than mode I. Furthermore, the requirement that r_u be equal to r_w may not be a physical one. These two facts together with the ambiguities of the model possibly explain the observed spread in parameter values.

3.5. ANALYSIS IN MODE III

Although the analysis performed in mode I gave satisfactory fits to the data, it seemed advisable to test whether observed trends were preserved when more than two parameters (as in the case of Co, ^{65}Cu, Au and ^{208}Pb) were allowed to vary. In this connection, it must be kept in mind that precisely the two parameters r_w and a_w, which were varied, show the greatest scatter in their values. On the other hand the results of a free five-parameter search such as mode II suggest that the ambiguities of the model may mask any underlying trends in the parameters.

It is obvious that, in order to prevent the occurrence of such ambiguities, simultaneous variation of certain parameters must be avoided. A guide as to which parameters had to be selected for variation is provided by a paper by Halbert [2]), from which fig. 6 has been taken. Fig. 6 confirms the well-known fact that variations of a single parameter are more effective in distorting the angular distribution at backward angles. Moreover, some changes affect only certain portions of the curve, depending on the sign of the slope. Table 2 summarizes the type of change in $\sigma_{th}(\theta)$ produced by a small positive variation of each parameter according to the slope of the angular distribution. Here O denotes practically no change. The diffuseness a_w has been excluded from the table since its pattern of distortion is too complex for this qualitative analysis.

Table 2 and fig. 6 show, for example, that the distortion produced by changes in W and r_w are very similar. Furthermore, one might reasonably expect that changes in one parameter can be compensated by proper variations in no more than two of

TABLE 2

Sign of the variation of $\sigma_{th}(\theta)$ due to a small positive change in a single parameter, according to the slope in the angular distribution

Slope	δU	δr_u	δa_u	δW	δr_w
> 0	+	0	−	+	+
< 0	−	−	−	0	0

the remaining parameters. For example, a change in r_u (see table 2) mainly affects the negative slopes. On the other hand, simultaneous changes in U and a_u would tend to cancel out the distortion of the positive slopes and reinforce variations on

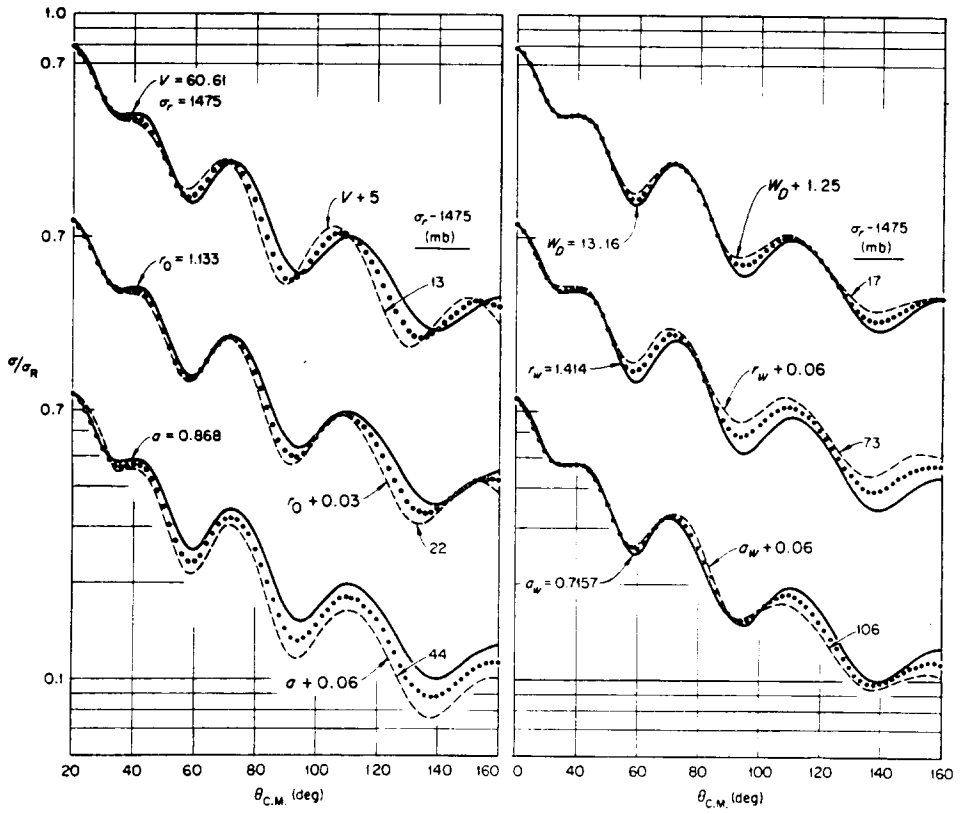

Fig. 6. Sensitivity of $\sigma_{th}(\theta)$ and σ_r to optical-model parameters, which is reproduced from Halbert[2]). The dashed curves show how σ_{th}/σ_R changes when each of the six parameters is varied separately. For each parameter, the original and the altered values are marked (in MeV or in fm). The dots indicate σ_{th}/σ_R for a change in parameter just half of the marked change. The change in σ_r is indicated for each parameter change. In this paper's notation, $U = V$; $r_u = r_0$; $a_u = a$; $w = w_D$. Halbert uses a Saxon-derivative form factor for the imaginary potential.

the negative slopes of the angular distribution, thus leading to an over-all change in the curve similar to that due to a variation in r_u. This is just one case from quite a few relations concerning three parameters that can be extracted from table 2. They can be written symbolically as follows:

$$\delta U \simeq \delta r_u + \delta r_w, \tag{4}$$

$$\delta r_u \simeq \delta U + \delta a_u, \tag{5}$$

$$\delta a_u \simeq \delta r_u - \delta r_w, \tag{6}$$

$$\delta W \simeq \delta U - \delta a_u, \tag{7}$$

$$\delta W \simeq \delta r_u - \delta a_u, \tag{8}$$

where $\pm\delta$ denotes plus or minus suitable small variation of and the symbol $\simeq$ should be read as "produces the same effects as". In addition, the two-parameter relation

$$\delta W \simeq \delta r_w \tag{9}$$

should also be considered.

If such "second order" ambiguities really exist, one should not simultaneously vary any three parameters appearing in each of the relations (4)–(8). On the basis of these ideas, the parameters chosen for variation on mode III were a_u, r_w and a_w. These parameters also showed unsatisfactory trends as resulting from mode I. Further variation of any two of the remaining parameters led only to slight modifications of them with no significant improvement of the fits. This can be taken as an incidental confirmation of the unambiguity of the parameters chosen for variation.

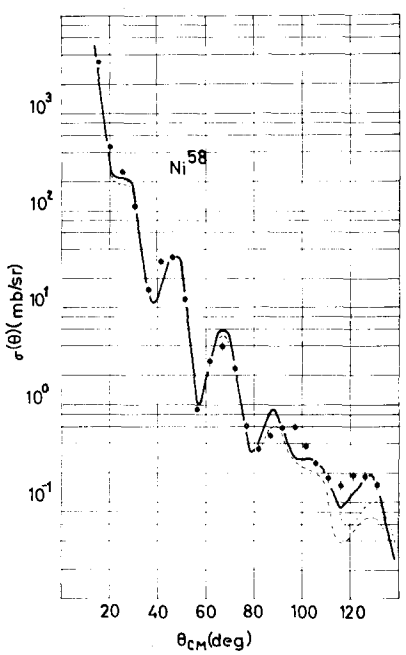

Fig. 7. Fit to the ^{58}Ni data in the one-nucleon family (dashed curve). The full line represents the optical model predictions in mode I, whereas the dotted curve is the one-nucleon family fit to those predictions.

The final values obtained in mode I were taken as initial ones for mode III. The results are also displayed in table 1 and figs. 2, 3 and 5. Their behaviour, both in goodness of fit and trends with atomic number, is very similar to that of mode I.

3.6. THE ONE-NUCLEON FAMILY

A few searches were carried out on ^{58}Ni and ^{59}Co data using potentials similar to those encountered in one-nucleon analyses. Good fits to the data were obtained only at the cost of allowing abnormally low values of the radius parameter. In addition to the usual fits to the experimental data a test was made of the ambiguity between both families.

To this end, the predictions obtained from mode I for ^{58}Ni were taken as experimental data in the search programme. A good fit to these data was sought, and the search was biassed so that the radius parameter would not become too small. The convergence of the search was very slow, and the resulting fit rather poor. When the requirement on the radius was removed the search became rapidly convergent to a good fit. The resulting fits are shown in fig. 7 and the corresponding parameters appear in table 3. It may be seen that discrepancies between both families appear

TABLE 3

Optical parameters for the one-nucleon family

Nucleus	U (MeV)	r_u (fm)	a_u (fm)	W (MeV)	r_w (fm)	a_w (fm)	ξ^2	σ_r (mb)
^{59}Co	73.35	0.87	1.10	17.03	1.28	1.69	15.3	1551
^{59}Co	61.85	0.98	1.04	16.81	1.28	1.69	16.1	1551
^{58}Ni	58.65	1.03	1.03	14.49	1.32	1.58	14.8	1503
^{58}Ni	58.65	1.03	1.03	14.49	1.32	1.58	10.7	1503 [a]
^{58}Ni	60.694	1.0272	1.039	16.067	1.33	1.539	4.9	1512 [a]
^{58}Ni	35.59	1.37	0.643	11.03	1.285	1.90	22.3	1550 [b]

[a]) Search made trying to fit the optical model predictions of mode I.

[b]) As in a), but the search was biassed to avoid too low values of the radius parameter.

only at backward angles, where the influence of other effects not taken into account in this work, such as spin-orbit coupling and channel coupling also become important. This strengthens the belief that a choice between the two families from scattering data alone is practically impossible.

3.7. TOTAL REACTION CROSS-SECTIONS

Values of total reaction cross-sections at a similar energy have been obtained by Mayo *et al.* [6]) in an independent experiment. Their values, together with the optical model predictions, appear in table 1 and are plotted in fig. 8. The points marked with error bars are experimental results. They show a regular behaviour, although there are two regions in the vicinity of nickel and tin with an indication of a dip in the cross-sections. The optical model predictions show a similar but less pronounced dip in the nickel region. These were also observed for protons at various energies [15]) and are possibly associated with the presence of proton closed shells corresponding to

atomic numbers $Z = 28$ and $Z = 50$. The optical model cross-sections depend very little on the mode of analysis for light and medium-weight nuclei.

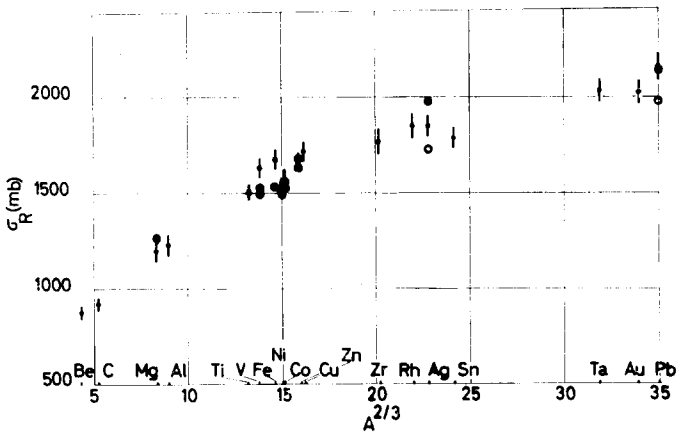

Fig. 8. Total reaction cross-sections as measured by Mayo *et al.* [6]) at 26.5 MeV and optical model predictions from the present scattering data. Symbols correspond to those of fig. 2.

The latter result does not apply to heavy nuclei. This may be due to the fact that the angular distributions, having no pronounced structure, are equally well fitted by widely different reflection coefficients.

The authors are indebted to Dr. L. C. Gomes for making available his results on the deuteron potential prior to publication. They express their gratitude to Dr. P. E. Hodgson for many fruitful discussions during his stay in Buenos Aires and for providing the optical model programme used in the calculations. Thanks are also due to Mr. H. O. Conde and the synchrocyclotron crew for their able assistance during the experiment.

References

1) G. Igo and R. M. Thaler, Phys. Rev. **106** (1957) 126;
G. Igo, Phys. Rev. Lett. **1** (1958) 167;
M. A. Melkanoff, T. Sawada and N. Cindro, Phys. Lett. **2** (1962) 98
2) E. C. Halbert, Nuclear Physics **50** (1964) 353
3) C. M. Perey and F. G. Perey, Phys. Rev. **132** (1963) 755
4) H. R. E. Tjin A Djie, F. Udo and L. A. Ch. Koerts, Nuclear Physics **53** (1964) 625;
P. T. Andrews *et al.*, Nuclear Physics **56** (1964) 422;
J. Testoni, S. Mayo and P. E. Hodgson, Nuclear Physics **50** (1964) 479
5) R. Beurtey, R. Maillard, A. Papineau and J. Thirion, Compt. Rend. **257** (1963) 1477
6) B. D. Wilkins and G. Igo, Phys. Lett. **3** (1962) 48;
S. Mayo, W. Schimmerling, M. J. Sametband and R. M. Eisberg, Nuclear Physics **62** (1965) 393
7) R. M. Drisko, G. R. Satchler and R. H. Bassel, Phys. Lett. **5** (1963) 347
8) P. T. Andrews, R. W. Clifft, L. L. Green and J. F. Sharpey-Schafer, Nuclear Physics **56** (1964) 449

9) K. W. Brockman, Jr., Proc. Int. Symptosium on Direct Interactions and Nuclear Reaction Mechanisms, ed. by E. Clementel and C. Villi (Gordon and Breach, London, 1963) p. 159
10) R. N. Maddison, Proc. Phys. Soc. **79** (1962) 264
11) A. M. Lane, Revs. Mod. Phys. **29** (1957) 193
12) F. G. Perey, Phys. Rev. **131** (1963) 745
13) L. R. B. Elton, Nuclear sizes (Oxford University Press, London, 1961) p. 31
14) L. C. Gomes, private communication
15) K. Bearpark and W. R. Graham, Nuclear Physics Laboratory, University of Oxford Report No. 149–64